

Systematic study of $^{192,202,206,210}\text{Po}$ compound nuclei using neutron multiplicity as a probeRuchi Mahajan,^{*} B. R. Behera,[†] Meenu Thakur, Gurpreet Kaur, Priya Sharma, Kushal Kapoor, and A. Kumar
*Department of Physics, Panjab University, Chandigarh 160014, India*P. Sugathan, A. Jhingan, A. Chatterjee, N. Saneesh, A. Yadav, and R. Dubey
*Inter University Accelerator Centre, Aruna Asaf Ali Marg, New Delhi 110067, India*Neeraj Kumar
*Department of Physics and Astrophysics, University of Delhi 110067, India*Hardev Singh
*Department of Physics, Kurukshetra University, Kurukshetra 136119, India*A. Saxena
*Nuclear Physics Division, Bhabha Atomic Research Centre, Mumbai 400085, India*Santanu Pal[‡]
CS-6/1, Golf Green, Kolkata 700095, India (Received 23 September 2017; revised manuscript received 15 January 2018; published 4 September 2018)

In the present work we have measured pre- and post-scission neutron multiplicities (M_{pre} and M_{post}) from two compound nuclei, namely $^{192,202}\text{Po}$ populated by $^{48}\text{Ti} + ^{144,154}\text{Sm}$ systems at 72 MeV of excitation energy using the National Array of Neutron Detectors (NAND) facility at IUAC, New Delhi. Statistical model analysis has been performed for $^{48}\text{Ti} + ^{144,154}\text{Sm}$ along with already existing data for $^{12}\text{C} + ^{194}\text{Pt}$ and $^{18}\text{O} + ^{192}\text{Os}$ covering compound nuclei of Po ($^{192,202,206,210}\text{Po}$) with neutron number $N_C = 108, 118, 122, \text{ and } 126$ respectively. Variation of experimental M_{pre} with N/Z of the compound nucleus does not show any special feature at neutron shell closure ($N_C = 126$) at compound nucleus excitation energy around 72 MeV considered here. In particular, it is found that dissipation alone is unable to reproduce the experimental M_{pre} for ^{192}Po , and the role of entrance channel dynamics should be considered in future works.

DOI: [10.1103/PhysRevC.98.034601](https://doi.org/10.1103/PhysRevC.98.034601)**I. INTRODUCTION**

Fusion-fission of heavy nuclei is a complex dynamical process in which many degrees of freedom are involved. Though many aspects of this process have been investigated both qualitatively and quantitatively in the past, it is yet to be fully understood [1]. Following the capture of a projectile by a target nucleus, a compound nucleus (CN) is usually formed after complete equilibration in all the degrees of freedom. Subsequently the CN de-excites by competing processes of evaporation of light particles and photons, and fission. Sometimes the dinuclear system may segregate prematurely before forming a fully equilibrated CN. Such events with various degrees of equilibration appear between deep-inelastic collisions (DICs) and complete fusion [2]. In DIC, the entrance channel mass asymmetry is approximately preserved but there can be large dissipation of kinetic energy and angular momentum. CN

formation, in contrast, is characterized by equilibration of all degrees of freedom, and hence complete loss of identity of the entrance channel. Intermediate between DIC and CN fission, quasifission (QF) has full energy dissipation but incomplete drift toward the energetically favored mass-symmetric configuration [3–12].

It has been shown earlier from analyses of a large volume of experimental data from fusion-fission reactions that the multiplicities of different types of evaporation species are larger compared to the standard statistical model (SM) predictions [13,14]. This excess yield of particles and γ rays from heavy compound systems suggests a slowing down of the fission process as given by the transition-state model of fission [15]. The slowing down of the fission process or fission hindrance can be described by incorporating nuclear dissipation and transient effects allowing for the buildup of the fission flux [16–18]. Phenomenologically, it was suggested by Blocki *et al.* [19] that nuclear dissipation at moderate excitation energies is one-body in nature and arises out of the collisions of the nucleons with the moving nuclear surface (wall formula) and also due to the exchange of nucleons between the two lobes when the nucleus has a dinuclear shape (window formula).

^{*}ruchimahajan4@gmail.com[†]Corresponding author: bivash@pu.ac.in[‡]Formerly with VECC, Kolkata.

However, in most of the analyses, the strength of the dissipation is used as an adjustable parameter in order to fit experimental data. Apart from nuclear dissipation, the fission timescale is also sensitive to the shell effects in fission barrier height and the density of nuclear levels [11,20]. The feasibility of synthesis of super heavy elements is based on the expectation of their stability against fission due to shell effects [21]. The shell effect in experimental observables in heavy-ion-induced fusion-fission reactions is thus presently an active field of research. Recently, Singh *et al.* [22,23] and Sandal *et al.* [24] studied the effect of shell closure by neutron multiplicity measurements for the compound nuclei $^{213,215,217}\text{Fr}$ and $^{210,212,214,216}\text{Rn}$. In the present work, experimental measurement of M_{pre} is extended over a wider range of N/Z and fissility (χ) for compound nuclei of Po isotopes. Here we have measured the M_{pre} for two systems: (i) $^{48}\text{Ti} + ^{144}\text{Sm}$ and (ii) $^{48}\text{Ti} + ^{154}\text{Sm}$ at 72 MeV excitation energy. In the present study, we also include the systems $^{12}\text{C} + ^{194}\text{Pt}$ and $^{18}\text{O} + ^{192}\text{Os}$ populating ^{206}Po and ^{210}Po respectively, for which experimental data for neutron multiplicity are already available [25,26]. The chosen systems span the neutron-deficient ^{192}Po ($N_C = 108$) to neutron-rich ^{210}Po ($N_C = 126$) compound nuclei. We also perform a detailed SM analysis for the four systems. This paper is organized as follows: The experimental details are described in Sec. II, followed by the strategy of the data analysis procedure and results in Sec. III. In Sec. IV, SM calculations are discussed. Finally, the results of the analysis are summarized and concluded in Sec. V.

II. EXPERIMENTAL DETAILS

The experiment was carried out using the 15 UD Pelletron + LINAC facility of IUAC, New Delhi. A pulsed beam of ^{48}Ti (beam current = 0.5 p nA) having a repetition rate of 250 ns, at laboratory energies of 260 and 230 MeV, was incident on the ^{144}Sm (enrichment = 93.7%) and ^{154}Sm (enrichment = 98.7%) targets of thickness 270 and 250 $\mu\text{g}/\text{cm}^2$ respectively. Each target was prepared by evaporating (using thermal evaporation technique) the target material on the carbon backing of 20 $\mu\text{g}/\text{cm}^2$ thickness, and further covered by a layer of carbon capping of thickness 5 $\mu\text{g}/\text{cm}^2$ [27]. The targets were placed at the center of a thin-walled spherical scattering chamber having a diameter of 1 m. The fragments produced from fission of CN were detected by a pair of multiwire proportional counters (MWPC1 and MWPC2) (6.4 in. \times 4.4 in.) [28] kept at the fission fragment folding angle of $\pm 60^\circ$. These detectors were kept at a distance of 30 cm away from the target position. The fission detectors were operated at a pressure of 4 mbar of isobutane gas. The detectors have a three-electrode geometry, in which a cathode is sandwiched between two position sensitive anodes. The time-of-flight (TOF) spectrum of the fragments gave a very fine separation of the fission fragments from target- and projectile-like particles. Figure 1 shows clear separation of fission like events from other events. The elastically scattered events were used to calibrate the TOF spectrum of the fission fragments. For the present experiment, position and time resolutions of 1.2 mm and 1 ns were obtained. Two passivated implanted planar silicon (PIPS) detectors were also placed inside the chamber at $\pm 13.5^\circ$ with

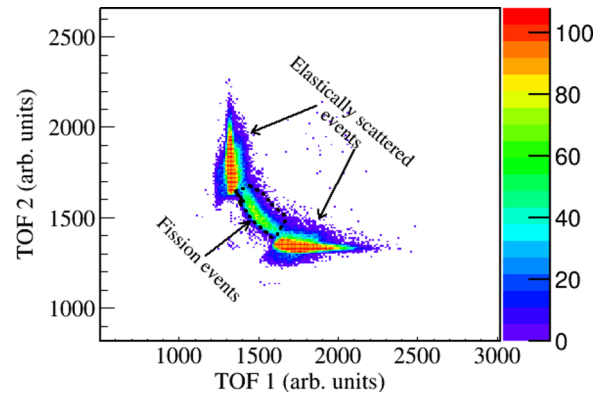


FIG. 1. Two-dimensional timing spectrum from the cathode of two MWPCs. Events corresponding to fission are marked with a black lobe.

respect to the beam direction for monitoring the beam. The neutrons emitted were detected in coincidence with the fission fragments by an array of organic liquid scintillators (BC501 A) [29,30]. It comprises 100 neutron detectors installed on a fixed-radius semisphere configuration. Each neutron detector has a cylindrical shape of dimensions 5 in. \times 5 in. These detectors are further coupled to a 5 in. photomultiplier tube (PMT Model Hamamatsu R4144). The detectors are housed on a geodesic dome structure containing detectors both in and out of the reaction plane. These detectors have a fixed flight path of 175 cm from the target. The dome is truncated 80 cm above the floor level. The dome has 111 vertices with circular hubs attached to each vertex and 100 detectors are distributed among these hubs. Eight rings are formed in this structure, the lowest ring being 15° below the reaction plane. The total solid angle coverage of the neutron detector array is 3.3% of 4π in this geometry. Out of these 100 detectors, 16 detectors were kept in the reaction plane (ranging from 18° to 342°) and the remaining 84 detectors were positioned out of the reaction plane for the present experiment. A schematic diagram, depicting experimental arrangement of the NAND chamber along with the in-plane neutron detectors, is shown in Fig. 2. Hardware thresholds for the neutron detectors were adjusted to 120 keV equivalent-electron (keVee) neutron energy using standard γ ray sources ^{137}Cs , ^{22}Na , and ^{60}Co [31]. The data acquisition was triggered by setting up a coincidence between RF of the beam pulse and any one of the MWPCs. The data selection was performed by gating the neutron energy spectra with the central lobe (fission-like events) as depicted in Fig. 1 so that other events were eliminated from the analysis. The fission-like events in the central lobe consist of pure fusion-fission events and also an admixture of QF and fast fission events. The data in the event mode were collected using a VME-based data acquisition system based on LAMPS software. The ion beam after the reaction on target was stopped beyond the detector array on a beam dump located at a distance of 4 m away from the target. This ion beam can further initiate secondary radiation including fast neutrons from the dump. In order to limit this background radiation reaching the neutron detectors, proper shielding of the beam dump was built using borated paraffin blocks and lead sheets surrounding the dump [32]. In order to

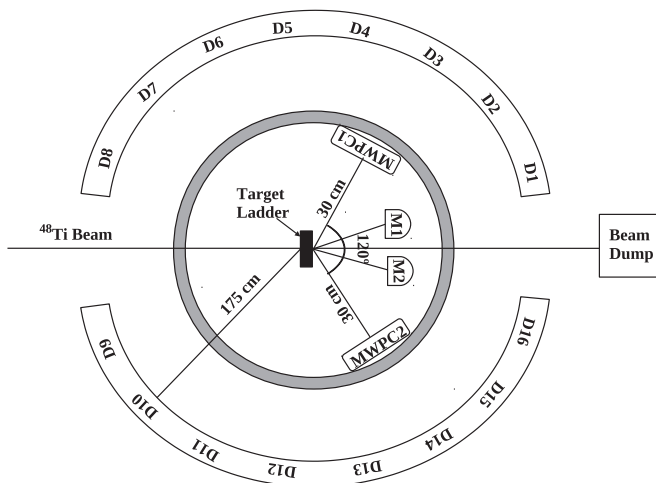


FIG. 2. Schematic diagram of the experimental setup. Detectors numbered from D1 to D16 refer to the neutron detectors present in the reaction plane. M1 and M2 are PIPS detectors used for beam monitoring.

monitor the beam pulsing, a BaF₂ detector was placed close to the beam dump. The pulse width of the beam was found to be 580 ps.

III. DATA ANALYSIS AND RESULTS

The main aim of this analysis is to extract pre- and post-scission components of neutron multiplicity. The data analysis part comprises the following steps:

A. Neutron detection efficiency

For experiments aiming to extract neutron multiplicity, the precise knowledge of detector efficiency is essential, as it will be used for correcting observed fission counts. In order to measure the neutron detection efficiency, ^{252}Cf was placed at the center of the reaction chamber of NAND [33]. ^{252}Cf decays by spontaneous fission and emits on an average 3.76 neutrons per fission. The intrinsic efficiency of BC501A detectors has been determined by the TOF technique. In measurements with the fission detector, a MWPC having dimensions 8 in. \times 4 in. was used. The detector was placed very close to the source (2 cm or closer). The MWPC timing signal provided the START while the STOP signal was taken from the neutron detector. The neutron energy spectrum from spontaneous fission of ^{252}Cf in the center-of-mass (CM) frame is well described by a Maxwellian distribution function given by the equation [34]

$$g(E)dE = 2 \frac{\sqrt{E}}{\sqrt{\pi}T^{3/2}} \exp\left(-\frac{E}{T}\right) \quad (1)$$

where E is neutron energy and T is the temperature of the neutron source, which is considered to be 1.42 MeV [34]. Knowing the number of fission F_n , the neutron multiplicity M_n , the solid angle Ω subtended by the neutron detector to the source position, and the distribution function $g(E)$, the number of neutrons impinging the detector in the CM frame

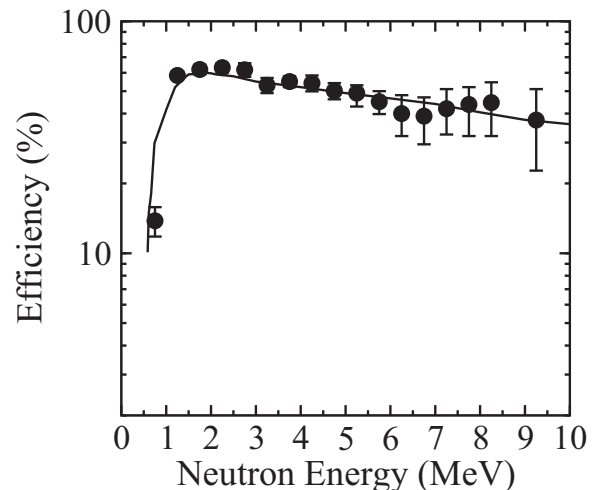


FIG. 3. Comparison of the experimentally deduced neutron efficiency (filled circle) with the one obtained using Monte Carlo simulation code FLUKA (solid line)

can be calculated as

$$\frac{dN}{dE} = F_n \times M_n \times \frac{\Omega}{4\pi} \times g(E)dE. \quad (2)$$

Since the fission detector has a wide angular coverage, the consequence of kinematic focusing on energy and counts can be neglected in the energy spectrum, though it is present for individual events. Assuming the fission detector detects fission fragments emitted in all the directions, the laboratory energy distribution of neutrons will coincide with CM energy distribution, and then the ratio of the two will give the intrinsic efficiency. Thus obtained efficiencies were then compared with the Monte Carlo simulated values from the FLUKA particle transport and interaction code [35]. The experimental observed efficiencies are in good agreement with the FLUKA simulated values as shown in Fig. 3.

B. Conversion of TOF spectra to neutron energy spectra

Since neutron detectors are sensitive to both γ rays and neutrons, the discrimination was done by pulse shape discrimination (PSD) based on zero crossover and the TOF technique using IUAC made PSD modules [36]. TOF spectra were calibrated using a precision TAC calibrator and the prompt γ -ray peak as reference. To distinguish the neutrons from γ rays, a two-dimensional neutron gate (PSD vs TOF) was applied over the calibrated TOF spectra. Figure 4 shows the two-dimensional plot of TOF vs PSD for one of the neutron detectors. The calibrated and gated TOF spectra were converted into the neutron energy (E_n) spectra. The neutron energy spectra were further corrected with the above obtained efficiency from the FLUKA simulation program.

C. Extraction of neutron multiplicity

A multiple-source least-square fitting procedure followed by a χ^2 minimization procedure was used to extract the pre- and post-scission components (M_{pre} and M_{post}) of neutron mul-

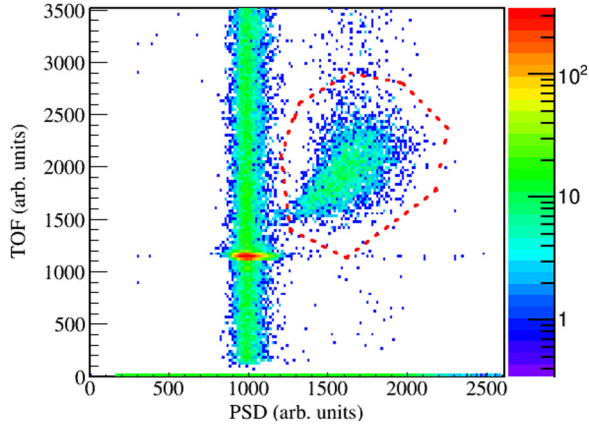


FIG. 4. TOF versus PSD spectrum for $^{48}\text{Ti} + ^{144}\text{Sm}$ reaction at 260 MeV. The neutron lobe is marked in red.

multiplicities and temperatures (T_{pre} and T_{post}) from the measured neutron energy spectra. The Watt expression [13] used for fitting procedure is given as

$$\frac{d^2M}{dE_n d\Omega_n} = \sum_{i=1}^3 \frac{M_i \sqrt{E_n}}{2(\pi T_i)^{3/2}} \times \exp \left[-\frac{E_n - 2\sqrt{E_n E_i / A_i} \cos \theta_i + E_i / A_i}{T_i} \right]. \quad (3)$$

Three moving sources of neutrons were considered: neutrons emitted from the CN, which correspond to pre-scission neutron emission (M_{pre}), and neutrons emitted from two fully accelerated fission fragments (FFs), which correspond to post-scission neutron emission (M_{post}). The neutrons emitted from these moving sources were assumed to be isotropic in their respective rest frames. Thus, the total neutron multiplicities can be written as the sum

$$M_{\text{total}} = M_{\text{pre}} + 2 \times M_{\text{post}}. \quad (4)$$

Here, E_n refers to the energy of neutrons in laboratory frame and A_i , E_i , T_i , and M_i are the mass, energy, temperature, and multiplicity of each neutron emitting source i . θ_i is the angle of a neutron with respect to the neutron emitting source. FF energies and folding angles were obtained from Viola systematics [37]. In order to avoid any angular uncertainty, the MWPC was divided into four equal slices each having dimension 36 mm \times 96 mm. The slicing of the MWPC is done in such a way that each neutron spectrum acquires sufficient statistics. Then, simultaneous fitting of 400 neutron energy spectra is performed keeping M_{pre} , M_{post} , T_{pre} , and T_{post} as free parameters. The temperature of the fissioning nucleus, T_{pre} was

calculated as

$$T_{\text{pre}} = \sqrt{E^*/a}, \quad (5)$$

where E^* is the CN excitation energy and a is the level density parameter, by assuming a to be $A_{\text{CN}}/10 \text{ MeV}^{-1}$. T_{pre} was scaled down to $(11/12)T$ to account for the cascade of sequential particle evaporation [38]. Neutron multiplicities obtained from fitting of decay of $^{192,202}\text{Po}$ are given in Table I, and the fitted plots are shown in Figs. 5 and 6 respectively.

It may be mentioned here that M_{pre} from the $^{48}\text{Ti} + ^{144}\text{Sm}$ reaction is possibly slightly overestimated due to the following reason. The ^{144}Sm target used in the present experiment was less enriched compared to the ^{154}Sm target. To set an upper limit to the systematic error in ^{154}Sm from ^{192}Po due to the presence of heavier Sm isotopes in the target, we may use the neutron multiplicity from ^{202}Po as the additional contribution to the measured numbers. Taking the larger fusion cross section of $^{48}\text{Ti} + ^{154}\text{Sm}$ compared to $^{48}\text{Ti} + ^{144}\text{Sm}$ into account and also the larger neutron multiplicity from ^{202}Po compared to that of ^{192}Po , the upper limit of contribution of the heavier isotopes in the measured neutron multiplicity for $^{48}\text{Ti} + ^{144}\text{Sm}$ is estimated to be about 6%. Nevertheless, it is also observed that M_{pre} from ^{192}Po CN is substantially smaller than those from the other heavier Po isotopes. This is because proton evaporation is also a competing channel for the highly neutron deficient ^{192}Po due to its relatively higher neutron binding energy compared to the heavier Po isotopes.

The experimental M_{pre} values are given as a function of N/Z for different Po isotopes in Fig. 7. For comparison, M_{pre} for three Fr isotopes are also shown. In both the cases, the general trend of M_{pre} is found to increase with N/Z . No specific trend in the data is indicated that might be identified with the effect of shell closure at $N=126$ (for ^{210}Po and ^{213}Fr). This, however, is not unexpected since shell effects become small at the excitation energies considered here. In particular for the Po isotopes, the CN decay mode changes predominantly from fission (for ^{192}Po) to evaporation for ($^{206,210}\text{Po}$) and this can further obscure any discernible effect of shell closure in experimental data.

The experimentally obtained total neutron multiplicities (M_{total}) were also compared with the energy balance equation following the prescription suggested by Hinde *et al.* [26]. In this procedure, two different methods were used to calculate the available decay energy of a CN; one of them is based on the excitation energy of the CN in the initial stage. Here, the total available decay energy is given as

$$E_x(f) = E_{\text{CM}} + Q(f) - E_K, \quad (6)$$

where E_{CM} is the energy in center-of-mass frame, $Q(f)$ is the Q value of the fission reaction, and E_K is the total kinetic energy of the FF. In the other method, the total available decay

TABLE I. Fitted values of M_{pre} , M_{post} , T_{pre} , T_{post} , and χ^2/NDF for $^{192,202}\text{Po}$, respectively.

System	M_{pre}	$2M_{\text{post}}$	M_{total}	T_{pre}	T_{post}	χ^2/NDF
$^{48}\text{Ti} + ^{144}\text{Sm} \rightarrow ^{192}\text{Po}$	1.92 ± 0.18	2.80 ± 0.12	4.72 ± 0.19	1.93 ± 0.15	1.45 ± 0.07	2.1
$^{48}\text{Ti} + ^{154}\text{Sm} \rightarrow ^{202}\text{Po}$	2.90 ± 0.20	3.28 ± 0.10	6.18 ± 0.22	1.78 ± 0.097	1.12 ± 0.04	1.9

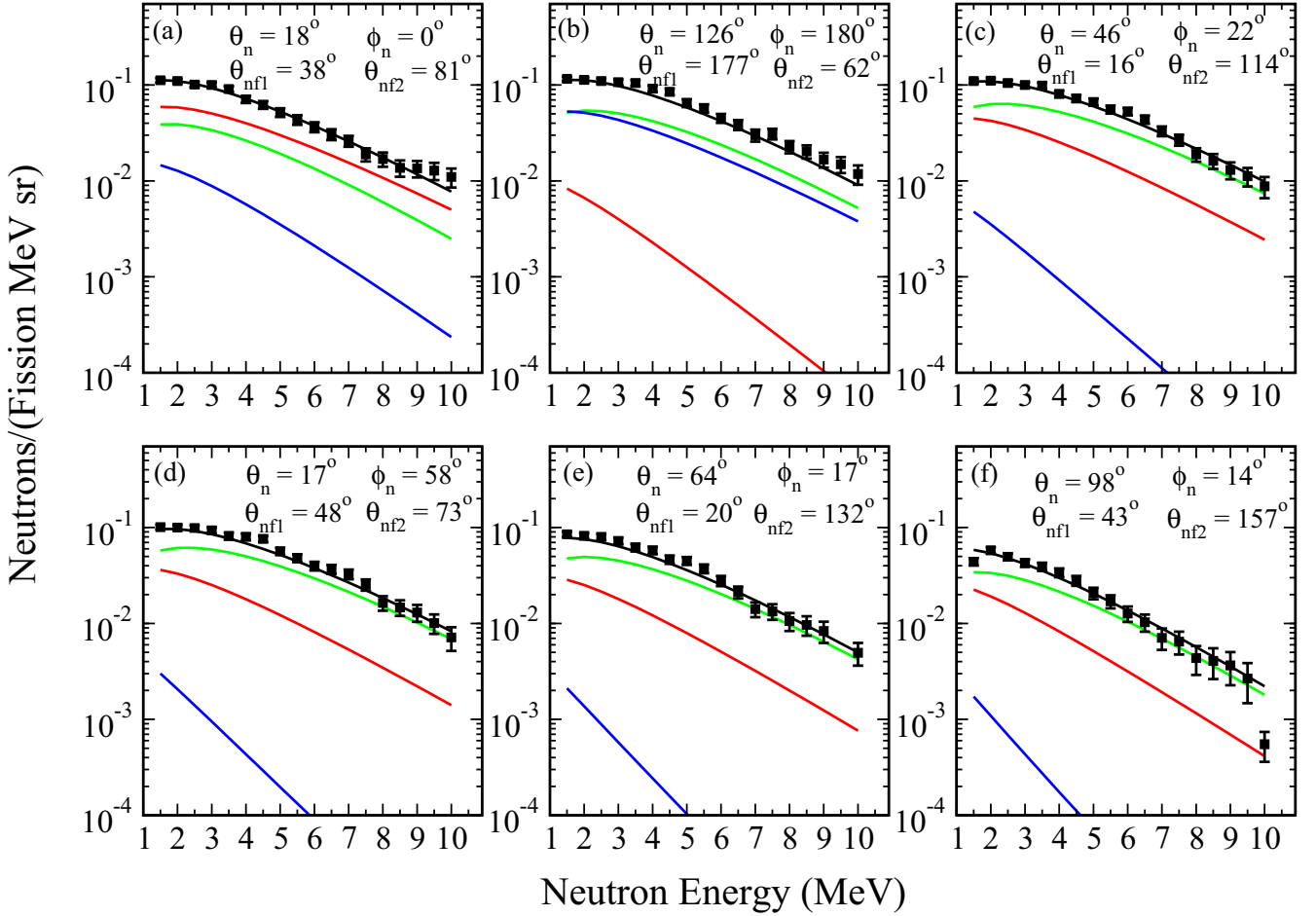


FIG. 5. (a)–(f) Neutron multiplicity spectra for the $^{48}\text{Ti} + ^{144}\text{Sm}$ system at 72 MeV excitation energy for six of the neutron detectors. The fits for the pre-scission (red line) and post-scission contributions from one fragment (blue line) and that from the other (green line) are shown. The solid black line represents the sum of the different contributions. Here, θ_n and ϕ_n refer to the polar and azimuthal angles of the neutron detectors whereas θ_{nf1} and θ_{nf2} are the relative angles between neutrons emitted and the fission fragments.

energy is obtained from the experimentally obtained M_{total} as

$$E_x(f) = E_\gamma(f) + \sum_{i=1}^{M_{\text{total}}} (8.07 + E_n^i), \quad (7)$$

where $E_\gamma(f)$ accounts for the excitation energy carried away by the emitted γ rays, 8.07 is the mass defect of a neutron in MeV, and E_n^i is the kinetic energy of the i th emitted neutron. The total available decay energies obtained by both the procedures for both the systems match within ± 5 MeV, which indicates the consistency of the experimentally measured multiplicities.

IV. THEORETICAL CALCULATIONS

The experimental values of M_{pre} and M_{post} are next compared with the SM predictions for the CN ^{192}Po and ^{202}Po populated through the $^{48}\text{Ti} + ^{144,154}\text{Sm}$ reactions. We also perform SM calculations for the CN ^{206}Po and ^{210}Po at excitation energies close to those of the present systems for which experimental values of M_{pre} are available in the literature [25,26]. We assume in the SM calculation that the whole of

the incident flux leads to CN formation (noncompound nuclear processes such as QF are not considered here). The CN can either undergo fission or reduce to a evaporation residue along with the emission of light particles—like neutrons, protons, α particles and γ rays. The dominant fission mode is assumed to be symmetric and the fission width Γ_{BW} is obtained from the transition-state model of fission due to Bohr and Wheeler [15]. The particle and γ -ray emission widths are obtained from the Weisskopf formula as given in [18]. A phase-space factor due to collective motion in the ground state is also included in Γ_{BW} [39]. The computer code VECSTAT is used for the statistical model analysis in the present work [40].

We obtain the fission barrier in the present calculation by including shell correction in the liquid-drop nuclear mass [41]. The shell correction term δ is defined as the difference between the experimental and the liquid-drop model (LDM) masses ($\delta = M_{\text{experimental}} - M_{\text{LDM}}$). The fission barrier of a CN carrying angular momentum l is then given as

$$B_f(l) = B_f^{\text{LDM}}(l) - (\delta_g - \delta_s), \quad (8)$$

where B_f^{LDM} is the liquid-drop model fission barrier [42] and δ_g and δ_s are the shell correction energies for the ground state and

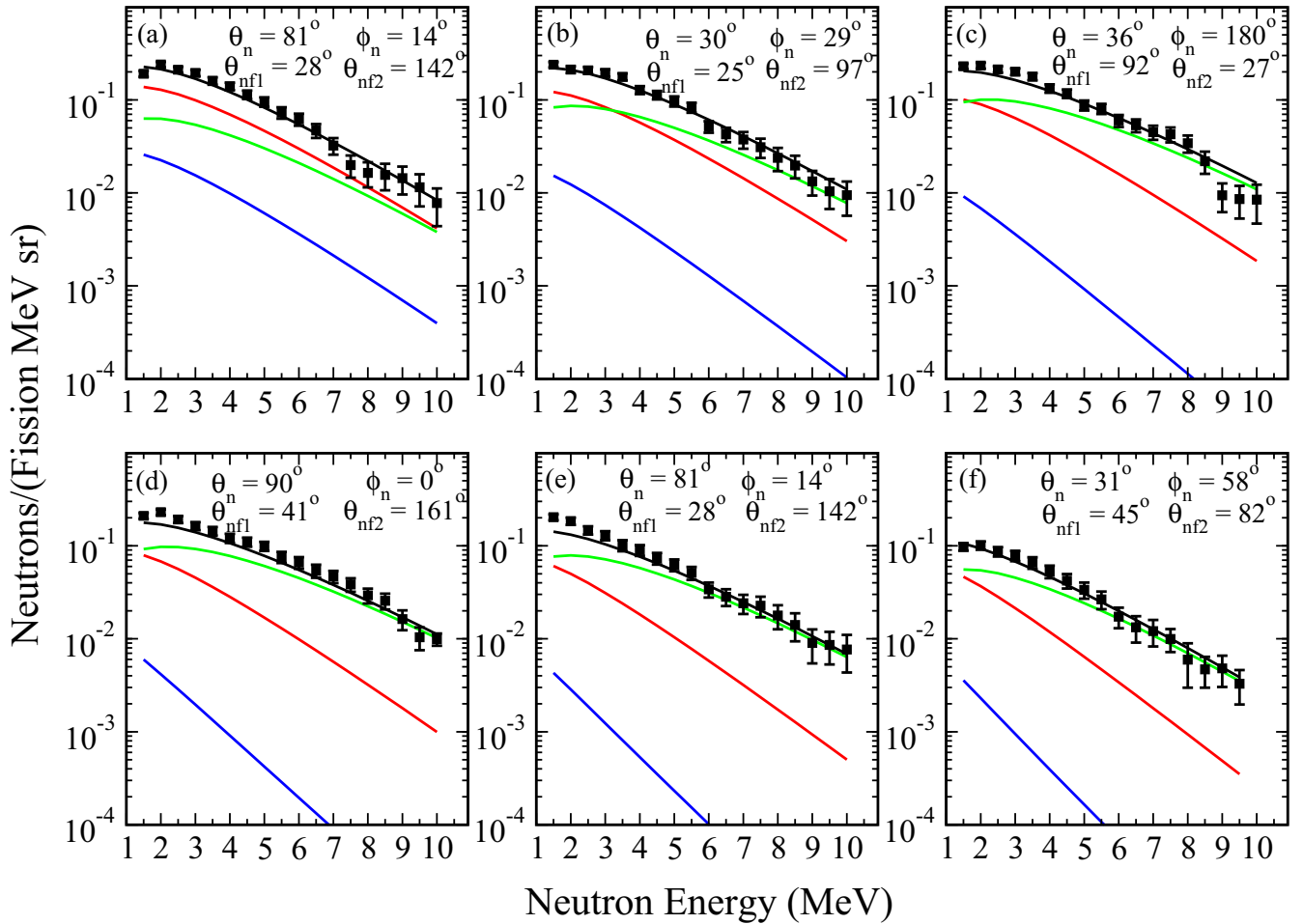


FIG. 6. (a)–(f) Neutron multiplicity spectra for the $^{48}\text{Ti} + ^{154}\text{Sm}$ system at 72 MeV excitation energy for six of the neutron detectors. The fits for the pre-scission (red line) and post-scission contributions from one fragment (blue line) and that from the other (green line) are shown. The solid black line represents the sum of the different contributions. Here, θ_n and ϕ_n refer to the polar and azimuthal angles of the neutron detectors whereas θ_{nf1} and θ_{nf2} are the relative angles between neutrons emitted and the fission fragments.

saddle configurations respectively. We obtain δ_g and δ_s by using the prescription given in Ref. [43] for deformation dependence of shell correction, which gives a very small value of shell correction at large deformations and full shell correction at zero deformation.

The shell effect is also considered in the nuclear level density, which is used to calculate various decay widths of the CN. For this purpose, we use the level density parameter from the work of Ignatyuk *et al.* [44], which includes shell effects at low excitation energies and goes over to its asymptotic form at high excitation energies. We use the shape-dependent asymptotic level density parameter as given by Reisdorf [45].

The spin distribution of the CN is an important ingredient of SM calculations and is obtained here from the coupled-channel code CCFULL using coupling constants and excitation energies of the low-lying collective states of both the projectile and the target nucleus. The depth parameter of the optical model potential for the (projectile-target) system is adjusted to reproduce the excitation function of fusion cross section. The resulting CN spin distribution is used as input to the SM calculation.

In the SM of CN decay, fission occurs when the CN crosses the saddle point. The number of neutrons emitted by the CN during its progression from the saddle to the scission configuration contributes to M_{pre} and is calculated using the saddle-to-scission transit time interval [46,47].

It may be noted that the fission cross sections of the four compound nuclei considered in the present study vary from very small (for ^{210}Po) to very large (for ^{192}Po) values. Hence, the SM predictions along with the experimental values of the M_{pre} are shown in Fig. 8 as a function of the fissility of the four compound nuclei $^{192,202,206,210}\text{Po}$. It is observed that SM underestimates the M_{pre} for all the cases.

This clearly indicates that a longer fission timescale or a fission hindrance is required in order to emit the experimentally observed number of pre-scission neutrons. A reduction in fission width can be obtained from a dissipative dynamical model of fission, where the Kramers-modified fission width is given as [48]

$$\Gamma_K = \Gamma_{\text{BW}} \left(\sqrt{1 + \left(\frac{\beta}{2\omega_s} \right)^2} - \frac{\beta}{2\omega_s} \right), \quad (9)$$

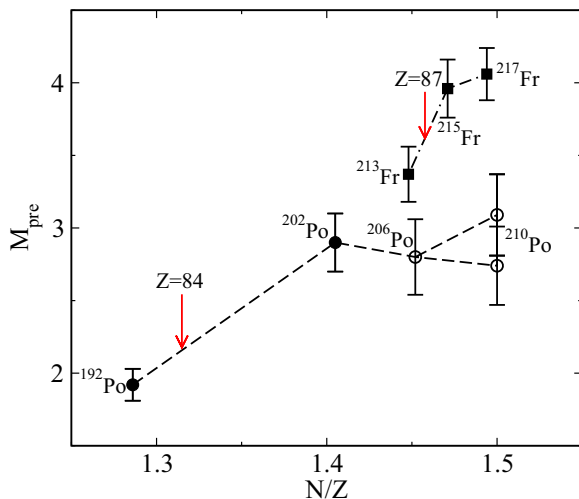


FIG. 7. M_{pre} as function of N/Z for Po ($Z = 84$) and Fr ($Z = 87$) isotopes. Present data are denoted by solid circles. Experimental values for ^{206}Po and ^{210}Po at excitation energies of 76.7 and 73.5 MeV are taken from [25] and [26] respectively and denoted by empty circles. Data (solid squares) for $^{213,215,217}\text{Fr}$ isotopes at excitation energies of 74.0, 75.4, and 74.0 MeV are taken from [22,23].

where Γ_{BW} is the Bohr-Wheeler fission width and β is the reduced dissipation coefficient (ratio of the dissipation coefficient to inertia). Dissipation also changes the saddle-to-scission time interval and is given as [46]

$$\tau_{ss} = \tau_{ss}^0 \left(\sqrt{1 + \left(\frac{\beta}{2\omega_s} \right)^2} + \frac{\beta}{2\omega_s} \right), \quad (10)$$

where τ_{ss}^0 is the saddle-to-scission transit time without any dissipation [46,47].

SM calculations are performed for different values of β and the variation of M_{pre} with β is given in Fig. 8. We find that while β values in the range $(10\text{--}20) \times 10^{21} \text{ s}^{-1}$ can reproduce the experimental multiplicities for the $^{18}\text{O} + ^{192}\text{Os}$ and $^{48}\text{Ti} + ^{154}\text{Sm}$ systems forming compound nuclei ^{210}Po and ^{202}Po respectively, a smaller value of β is required for the $^{12}\text{C} + ^{194}\text{Pt}$ system leading to the CN ^{206}Po . The range of the strength of the dissipation thus found is similar to the values used in earlier works [50,51]. However, for the $^{48}\text{Ti} + ^{144}\text{Sm}$ reaction forming the CN ^{192}Po , the number of pre-scission neutrons falls very short of the experimental value even with a strong dissipation of $\beta = 20 \times 10^{21} \text{ s}^{-1}$. Though a large fraction of M_{pre} is saddle-to-scission neutrons (M_{pre}^{ss}) for $\beta = 20 \times 10^{21} \text{ s}^{-1}$ ($M_{\text{pre}} = 1.27$ including $M_{\text{pre}}^{ss} = 0.44$), it is not large enough to explain the experimental multiplicity of 1.92 ± 0.18 . This indicates that the entrance channel dynamics may play some role in contributing to the number of pre-scission neutrons for the $^{48}\text{Ti} + ^{144}\text{Sm}$ system. The calculated total neutron multiplicity M_{total} values are, however, very close to the experimental values. The calculated M_{total} with $\beta = 10 \times 10^{21} \text{ s}^{-1}$ for the $^{48}\text{Ti} + ^{144,154}\text{Sm}$ systems are 4.51 and 5.71 while the experimental values are 4.72 ± 0.19 and 6.18 ± 0.22 respectively. The calculated values of M_{total} are nearly independent of the values of β .

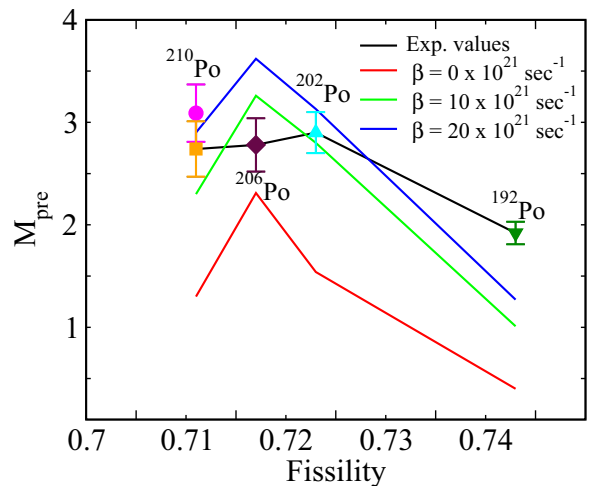


FIG. 8. M_{pre} as function of fissility [49] for different systems. The experimental values for $^{48}\text{Ti} + ^{144,154}\text{Sm} \rightarrow ^{192,202}\text{Po}$ (present work) are at excitation energies 72.6 and 72.3 MeV respectively, those of $^{12}\text{C} + ^{194}\text{Pt} \rightarrow ^{206}\text{Po}$ [25] and $^{18}\text{O} + ^{192}\text{Os} \rightarrow ^{210}\text{Po}$ [26] are at excitation energies 76.7 and 73.5 MeV respectively.

Another set of calculations are performed where a delay time (τ_{delay}) is introduced in the saddle-to-scission stage of fission in order to get a direct estimate of time delay required for emission of the experimentally observed number of pre-scission neutrons. This is an alternative to including dissipation in the calculation. The total saddle-to-scission transition time is then given as $(\tau_{ss}^0 + \tau_{\text{delay}})$. The τ_{delay} values required to reproduce the experimental M_{pre} are given in Fig. 9. We observe that τ_{delay} increases with fissility except for the CN ^{206}Po formed in the ($^{12}\text{C} + ^{194}\text{Pt}$) reaction. A possible explanation for this anomaly may be found if we compare the entrance channel mass asymmetry $\alpha = (A_T - A_P)/(A_T + A_P)$ with the critical Businaro-Gallone mass asymmetry α_{BG} [52] of the CN for different systems as shown in Table II. We note here that $\alpha < \alpha_{\text{BG}}$ for all the systems except for $^{12}\text{C} + ^{194}\text{Pt} \rightarrow ^{206}\text{Po}$, for which $\alpha > \alpha_{\text{BG}}$. It has been pointed out earlier that the fusion

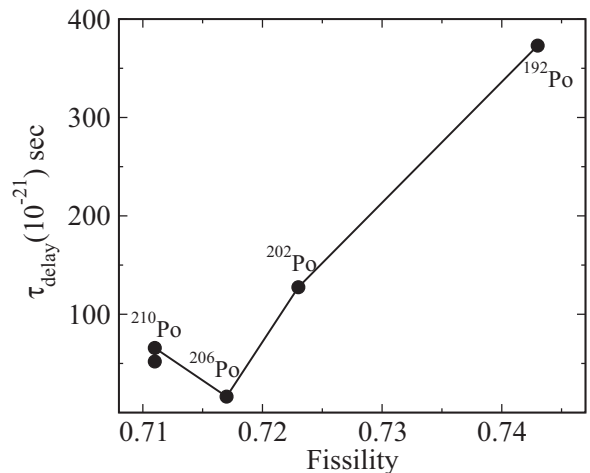


FIG. 9. τ_{delay} as function of fissility [49] for different systems.

TABLE II. Systems used in the present work.

System	E^* (MeV)	Expt. M_{pre}	χ	α	α_{BG}
$^{48}\text{Ti} + ^{144}\text{Sm} \rightarrow ^{192}\text{Po}$	72.6	1.92 ± 0.18	0.743	0.5	0.861
$^{48}\text{Ti} + ^{154}\text{Sm} \rightarrow ^{202}\text{Po}$	72.3	2.90 ± 0.20	0.723	0.525	0.851
$^{12}\text{C} + ^{194}\text{Pt} \rightarrow ^{206}\text{Po}$	76.7	2.8 ± 0.26	0.717	0.883	0.847
$^{18}\text{O} + ^{192}\text{Os} \rightarrow ^{210}\text{Po}$	73.5	$3.09/2.74 \pm 0.28/0.27$	0.711	0.829	0.844

path followed by a temperature equilibrated dinuclear system is quite different for systems with $\alpha > \alpha_{\text{BG}}$ than for those with $\alpha < \alpha_{\text{BG}}$ [49]. From a detailed analysis of several systems in the above work, it was further observed that the formation time, the time interval required to form a fully equilibrated CN, is smaller for systems with $\alpha > \alpha_{\text{BG}}$ than for those with $\alpha < \alpha_{\text{BG}}$. Since neutrons emitted during the formation time also contribute to the M_{pre} , fewer neutrons are expected to be emitted during the formation time and contribute to M_{pre} for the $^{12}\text{C} + ^{194}\text{Pt}$ reaction compared to the other systems. Consequently, τ_{delay} to reproduce the experimental M_{pre} for the $^{12}\text{C} + ^{194}\text{Pt}$ reaction can be smaller than the other systems, as we find in Fig. 9.

We point out here that experimental values of M_{pre} include neutrons emitted in three stages, namely (a) during the formation time, (b) during the time interval when the compound nucleus oscillates between the ground state and saddle configurations till it undergoes fission, and (c) during the transition of the CN from the saddle to the scission configuration. The present SM considers neutrons emitted during the stages (b) and (c) only, but not during (a). Thus the strength of the dissipation coefficient β when used as a fit parameter to reproduce experimental M_{pre} has also to account for the neutrons emitted during the formation time (a), though it is introduced to calculate the neutron number emitted in stages (b) and (c) only. This may lead to unusually large values of β when the formation time is large. Therefore, the observations for $^{48}\text{Ti} + ^{144}\text{Sm} \rightarrow ^{192}\text{Po}$ that very large β values are indicated in Fig. 8 and a large value of τ_{delay} in Fig. 9 suggest that the formation time for this system should be large in comparison to neighboring systems. This calls for a close look at the entrance channel dynamics of the above systems in future investigations.

The effect of QF events on neutron multiplicities has not been considered in the preceding discussions. Since the dinuclear complex in the entrance channel separates into projectile-like and target-like fragments before it attains full shape equilibration, the timescale of QF is expected to be smaller than those of compound nuclear fission. Consequently, the M_{pre} of QF events is also expected to be smaller than those from compound nuclear fission. Though QF events are expected to be more abundant in systems with higher symmetry in projectile and target masses [53], no evidence of QF has been observed in the excitation function of evaporation residue cross-section for $^{48}\text{Ti} + ^{144}\text{Sm}$ [54]. Similar observation was also made earlier for $^{48}\text{Ca} + ^{144}\text{Sm}$ [55]. Further, QF is not expected to be significant for the highly asymmetric $^{12}\text{C} + ^{194}\text{Pt}$ and $^{18}\text{O} + ^{192}\text{Os}$ systems. This leaves out only $^{48}\text{Ti} + ^{154}\text{Sm}$ reaction in the present work where QF events could contribute

to the experimental data. Hence, the present SM analysis (which does not consider QF) possibly over estimates M_{pre} for ^{202}Po . The contribution of QF in M_{pre} can, however, be resolved by gating over fission fragment masses [56,57], which is not considered in the present work. A distinguishing feature of $^{48}\text{Ti} + ^{144}\text{Sm}$ data presented here is the predominance of fast-fission events for which there is no LDM fission barrier.

Figure 10 shows the spin distribution of the compound nuclei ^{192}Po and ^{202}Po formed in $^{48}\text{Ti} + ^{144}\text{Sm}$ and $^{48}\text{Ti} + ^{154}\text{Sm}$ reactions. It is observed that a significant fraction of the ^{192}Po nuclei carrying large angular momentum faces no fission barrier and undergoes fast fission. Assuming the initial shape of the CN to be spherical, the transition time to reach scission configuration for all such events is obtained from Eq. (9), and the number of evaporated particles during this time interval is calculated in the present work. However, a better estimate of pre-scission multiplicities in fast fission should be obtained from dynamical models such as those employing Langevin equations [51].

In the present work, we have not considered neutrons that can be emitted during the accelerating phase of the fission fragments [58] and those from neck rupture [59]. We expect that inclusion of the above contributions would not change the systematic variation of β and τ_{delay} for CN in an isotopic chain. In fact, one may expect a smaller number of neutrons from neck rupture of a neutron-deficient CN ^{192}Po compared to the other Po isotopes considered here. This can widen the difference

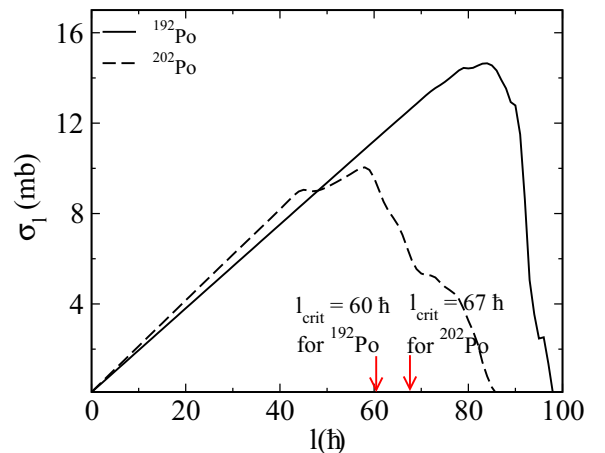


FIG. 10. The partial fusion cross-sections as function of CN spin. The excitation energies of ^{192}Po and ^{202}Po are 72.6 and 72.3 MeV respectively. The critical angular momentum l_{crit} where the LDM fission barrier vanishes is also marked for the two systems.

between the formation time of $^{48}\text{Ti} + ^{144}\text{Sm} \rightarrow ^{192}\text{Po}$ and the other reactions.

V. SUMMARY AND CONCLUSION

Pre- and post-scission neutron multiplicities have been measured for the $^{48}\text{Ti} + ^{144,154}\text{Sm}$ reactions populating the compound nuclei $^{192,202}\text{Po}$ at an excitation energy of 72 MeV. The total neutron multiplicities agree with the requirement of energy balance within 5%. Combining the present data with data from the literature [25,26] for ^{206}Po and ^{210}Po at similar excitation energies, pre-scission neutron multiplicities from Po compound nuclei with a wide range of neutron number ($N_C = 108$ to 126) are obtained. In the N/Z dependence of M_{pre} , no specific trend at shell closure of $N_C = 126$ is observed at CN excitation energy around 72 MeV. Shell effects are also not expected to survive at such high excitation energies. SM analyses with an adjustable strength of dissipation coefficient indicate that entrance channel effects (though not included in the present SM results) should be considered to account for M_{pre} . The CN ^{206}Po considered here is populated in the highly asymmetric $^{12}\text{C} + ^{194}\text{Pt}$ reaction, where shape equilibration in the entrance channel is expected to be fast. Consequently, the formation time of the CN would be small, resulting in fewer pre-scission neutrons and a smaller dissipation strength

to reproduce this number compared to the neighboring systems. On the other hand, M_{pre} for ^{192}Po could not be reproduced even with a very large value of the dissipation strength. Analysis with the introduction of a delay time in the SM calculation suggests that a substantial part of M_{pre} for the reaction $^{48}\text{Ti} + ^{144}\text{Sm} \rightarrow ^{192}\text{Po}$ may originate during CN formation in the entrance channel. However, SM analysis of M_{pre} for $^{48}\text{Ti} + ^{154}\text{Sm} \rightarrow ^{202}\text{Po}$ does not indicate any special role of the CN formation time. A comparative study of the entrance channel dynamics of the two systems will be useful to resolve this issue.

ACKNOWLEDGMENTS

The authors would like to thank the accelerator groups (LINAC and Pelletron) of IUAC, New Delhi for providing beams of excellent quality throughout the experiment. Help received from Mr. Abhilash in making thin enriched $^{144,154}\text{Sm}$ targets is acknowledged. We give special thanks to Prof. D. Mehta from Department of Physics, P.U. Chandigarh and Mr. Sunil Ohja of IUAC, New Delhi for providing the EDXRF and RBS facilities, respectively, for the characterization of these targets. One of the authors (R.M.) wants to acknowledge financial support from University Grants Commission (UGC), India in the form of a research fellowship. NAND project is funded by the Department of Science and Technology (DST), Government of India, under the Grant No. IR/S2/PF-02/2007.

-
- [1] C. J. Lin, R. du Rietz, D. J. Hinde, M. Dasgupta, R. G. Thomas, M. L. Brown, M. Evers, L. R. Gasques, and M. D. Rodriguez, *Phys. Rev. C* **85**, 014611 (2012).
- [2] R. Rafiei, R. G. Thomas, D. J. Hinde, M. Dasgupta, C. R. Morton, L. R. Gasques, M. L. Brown, and M. D. Rodriguez, *Phys. Rev. C* **77**, 024606 (2008).
- [3] W. Reisdorf and M. Schädel, *Physik A - Hadrons Nucei* **47**, 343 (1992).
- [4] W. J. Swiatecki, *Phys. Scr.* **24**, 113 (1981).
- [5] S. Bjornholm and W. J. Swiatecki, *Nucl. Phys. A* **391**, 471 (1982).
- [6] P. Moller and A. J. Sierk, *Nature (London)* **422**, 485 (2003).
- [7] W. U. Schroder and J. R. Huizenga, in *Damped Nuclear Reactions*, Treatise on Heavy-ion Science, edited by D. A. Bromley (Plenum, New York, 1984), Vol. 2, p. 115.
- [8] J. Töke, R. Bock, G. X. Dai, A. Gobbi, S. Gralla, K. D. Hildenbrand, J. Kuzminski, W. F. J. Müller, A. Olmi, H. Stelzer, B. B. Back, and S. Bjornholm, *Nucl. Phys. A* **440**, 327 (1985).
- [9] D. J. Hinde *et al.*, *J. Nucl. Radiochem. Sci.* **3**, 31 (2002).
- [10] S. Mitsuoka, H. Ikezoe, K. Nishio, K. Satou, and J. Lu, *Phys. Rev. C* **65**, 054608 (2002).
- [11] B. B. Back, D. J. Blumenthal, C. N. Davids, D. J. Henderson, R. Hermann, D. J. Hofman, C. L. Jiang, H. T. Penttila, and A. H. Wuosmaa, *Phys. Rev. C* **60**, 044602 (1999).
- [12] R. N. Sagaidak and A. N. Andreyev, *Phys. Rev. C* **79**, 054613 (2009).
- [13] D. Hilscher, J. R. Birkelund, A. D. Hoover, W. U. Schroder, W. W. Wilcke, J. R. Huizenga, A. C. Mignerey, K. L. Wolf, H. F. Breuer, and V. E. Viola, *Phys. Rev. C* **20**, 576 (1979).
- [14] M. Thoennessen and G. F. Bertsch, *Phys. Rev. Lett.* **71**, 4303 (1993).
- [15] N. Bohr and J. A. Wheeler, *Phys. Rev.* **56**, 426 (1939).
- [16] P. Frobrich and R. Lipperheide, *Theory of Nuclear Reactions* (Oxford University Press, Oxford, 1996).
- [17] Y. Abe, S. Ayik, P. G. Reinhard, and E. Suraud, *Phys. Rep.* **275**, 49 (1996).
- [18] P. Frobrich and I. I. Gontchar, *Phys. Rep.* **292**, 131 (1998).
- [19] J. Blocki, Y. Boneh, J. R. Nix, J. Randrup, M. Robel, A. J. Sierk, and W. J. Swiatecki, *Ann. Phys.* **113**, 330 (1978).
- [20] K. Mahata, S. Kailas, A. Shrivastava, A. Chatterjee, P. Singh, S. Santra, and B. S. Tomar, *Phys. Rev. C* **65**, 034613 (2002).
- [21] Y. Oganessian, *J. Phys. G: Nucl. Part. Phys.* **34**, 165 (2007).
- [22] V. Singh, B. R. Behera, M. Kaur, P. Sugathan, K. S. Golda, A. Jhingan, J. Sadhukhan, D. Siwal, S. Goyal, S. Santra, A. Kumar, R. K. Bhowmik, M. B. Chatterjee, A. Saxena, S. Pal, and S. Kailas, *Phys. Rev. C* **86**, 014609 (2012).
- [23] V. Singh, B. R. Behera, M. Kaur, A. Kumar, P. Sugathan, K. S. Golda, A. Jhingan, M. B. Chatterjee, R. K. Bhowmik, D. Siwal, S. Goyal, J. Sadhukhan, S. Pal, A. Saxena, S. Santra, and S. Kailas, *Phys. Rev. C* **87**, 064601 (2013).
- [24] R. Sandal, B. R. Behera, V. Singh, M. Kaur, A. Kumar, G. Singh, K. P. Singh, P. Sugathan, A. Jhingan, K. S. Golda, M. B. Chatterjee, R. K. Bhowmik, S. Kalkal, D. Siwal, S. Goyal, S. Mandal, E. Prasad, K. Mahata, A. Saxena, J. Sadhukhan, and S. Pal, *Phys. Rev. C* **87**, 014604 (2013).
- [25] G. G. Chubaryan, M. G. Itkis, S. M. Luk'yanov, V. N. Okolovich, Yu. E. Penionzhkevich, A. Ya. Rusanov, V. S. Salamatin, and G. N. Smirenkin, *Yad. Fiz.* **56**, 3 (1993) [*Phys. At. Nucl.* **56**, 286 (1993)].

- [26] D. J. Hinde, R. J. Charity, G. S. Foote, J. R. Leigh, J. O. Newton, S. Ogazac, and A. Chatterjee, *Nucl. Phys. A* **452**, 550 (1986).
- [27] R. Mahajan, S. R. Abhilash, P. Sharma, G. Kaur, D. Kabiraj, H. Duggal, D. Mehta, and B. R. Behera, *Vacuum* **150**, 203 (2018).
- [28] A. Jhingan, G. Kaur, N. Saneesh, R. Mahajan, M. Thakur, T. Banerjee, R. Dubey, P. Sharma, A. Yadav, R. Ahuja, B. R. Behera, and P. Sugathan, *Proc. DAE Symp. Nucl. Phys.* **60**, 936 (2015).
- [29] P. Sugathan, A. Jhingan, K. S. Golda, T. Varughese, S. Venkataramanan, N. Saneesh, V. V. Satyanarayana, S. K. Suman, J. Antony, R. Shanti, K. Singh, S. K. Saini, A. Gupta, A. Kothari, P. Barua, Rajesh Kumar, J. Zacharias, R. P. Singh, B. R. Behera, S. K. Mandal, I. M. Govil, and R. K. Bhowmik, *Pramana* **83**, 807 (2014).
- [30] K. S. Golda, A. Jhingan, P. Sugathan, H. Singh, R. P. Singh, B. R. Behera, S. Mandal, A. Kothari, A. Gupta, J. Zacharias, M. Archunan, P. Barua, S. Venkataramanan, R. K. Bhowmik, I. M. Govil, S. K. Datta, and M. B. Chatterjee, *Nucl. Instrum. Methods* **763**, 58 (2014).
- [31] T. G. Masterson, *Nucl. Instrum. Methods* **88**, 61 (1970).
- [32] N. Saneesh, M. Thakur, R. Mahajan, G. Kaur, R. Dubey, S. Venkataramanan, A. Jhingan, and P. Sugathan, *Proc. DAE Symp. Nucl. Phys.* **58**, 986 (2013).
- [33] N. Saneesh, A. Jhingan, and P. Sugathan, *Proc. DAE Symp. Nucl. Phys.* **60**, 1074 (2015).
- [34] *Proc. Advisory Group Mtg. Properties of Neutron Sources*, IAEA-TECDOC-410, International Atomic Energy Agency (1987).
- [35] A. Ferrari, P. R. Sala, A. Fasso, and J. Ranft, FLUKA: A Multi particle Transport Code, Reports No. CERN-2005-10, No. INFN/TC 05/11, and No. SLAC-R-773, 2005 (unpublished).
- [36] S. Venkataramanan, A. Gupta, K. S. Golda, H. Singh, R. Kumar, R. P. Singh, and R. K. Bhowmik, *Nucl. Instrum. Methods Phys. Res., Sect. A* **596**, 248 (2008).
- [37] V. E. Viola, K. Kwiatkowski, and M. Walker, *Phys. Rev. C* **31**, 1550 (1985).
- [38] E. Holub, D. Hilscher, G. Ingold, U. Jahnke, H. Orf, and H. Rossner, *Phys. Rev. C* **28**, 252 (1983).
- [39] V. M. Strutinsky, *Phys. Lett. B* **47**, 121 (1973).
- [40] J. Sadhukhan, Ph.D. thesis, Homi Bhabha National Institute, Mumbai, 2012 (unpublished).
- [41] K. Mahata, S. Kailas, and S. S. Kapoor, *Phys. Rev. C* **92**, 034602 (2015).
- [42] A. J. Sierk, *Phys. Rev. C* **33**, 2039 (1986).
- [43] W. D. Myers and W. J. Swiatecki, *Nucl. Phys.* **81**, 1 (1966).
- [44] A. V. Ignatyuk, G. M. Smirenkin, and A. Tishin, *Sov. J. Nucl. Phys.* **21**, 255 (1975).
- [45] W. Reisdorf, *Z. Phys. A* **300**, 227 (1981).
- [46] H. Hofmann and J. R. Nix, *Phys. Lett. B* **122**, 117 (1983).
- [47] P. Grangé, S. Hassani, H. A. Weidenmüller, A. Gavron, J. R. Nix, and A. J. Sierk, *Phys. Rev. C* **34**, 209 (1986).
- [48] H. A. Kramers, *Physica (Amsterdam)* **7**, 284 (1940).
- [49] A. Saxena, A. Chatterjee, R. K. Choudhury, S. S. Kapoor, and D. M. Nadkarni, *Phys. Rev. C* **49**, 932 (1994).
- [50] I. Dioszegi, N. P. Shaw, I. Mazumdar, A. Hatzikoutelis, and P. Paul, *Phys. Rev. C* **61**, 024613 (2000).
- [51] K. Mazurek, P. N. Nadtochy, E. G. Ryabov, and G. D. Adeev, *Eur. Phys. J. A* **53**, 79 (2017).
- [52] M. Abe, KEK Report No. 86-26, KEK TH-28, 1986 (unpublished).
- [53] B. B. Back, P. B. Fernandez, B. G. Glagola, D. Henderson, S. Kaufman, J. G. Keller, S. J. Sanders, F. Videbaek, T. F. Wang, and B. D. Wilkins, *Phys. Rev. C* **53**, 1734 (1996).
- [54] P. Sharma, B. R. Behera, R. Mahajan, M. Thakur, G. Kaur, K. Kapoor, K. Rani, N. Madhavan, S. Nath, J. Gehlot, R. Dubey, I. Mazumdar, S. M. Patel, M. Dhibar, M. M. Hosamani, Khushboo, N. Kumar, A. Shamlath, G. Mohanto, and S. Pal, *Phys. Rev. C* **96**, 034613 (2017).
- [55] G. N. Knyazheva, E. M. Kozulin, R. N. Sagaidak, A. Yu. Chizhov, M. G. Itkis, N. A. Kondratiev, V. M. Voskressensky, A. M. Stefanini, B. R. Behera, L. Corradi, E. Fioretto, A. Gadea, A. Latina, S. Szilner, M. Trotta, S. Beghini, G. Montagnoli, F. Scarlassara, F. Haas, N. Rowley, P. R. S. Gomes, and A. Szanto de Toledo, *Phys. Rev. C* **75**, 064602 (2007).
- [56] S. Appannababu, M. Cinausero, T. Marchi, F. Gramegna, G. Prete, J. Bermudez, D. Fabris, G. Collazuol, A. Saxena, B. K. Nayak, S. Kailas, M. Bruno, L. Morelli, N. Gelli, S. Piantelli, G. Pasquali, S. Barlini, S. Valdré, E. Vardaci, L. Sajo-Bohus, M. Degerlier, A. Jhingan, B. R. Behera, and V. L. Kravchuk, *Phys. Rev. C* **94**, 044618 (2016).
- [57] M. Thakur, B. R. Behera, R. Mahajan, N. Saneesh, G. Kaur, P. Sharma, R. Dubey, K. Kapoor, A. Yadav, N. Kumar, S. Kumar, K. Rani, P. Sugathan, A. Jhingan, A. Chatterjee, M. B. Chatterjee, S. Mandal, A. Saxena, S. Pal, S. Kailas, A. Nasirov, and B. Kayumov, *Eur. Phys. J. A* **53**, 133 (2017).
- [58] V. P. Eismont, *Sov. J. At. Energy* **19**, 1000 (1965).
- [59] N. Carjan and M. Rizea, *Phys. Lett. B* **747**, 178 (2015).